Technical Report of Predictive Active Steering Control for Autonomous Vehicle Systems

Charith Reddy GannapuReddy*, Raghu Dharahas Reddy Kotla†

***Abstract*—This study presents an analysis of a journal article on a model predictive control approach for active front steering control [1]. The assumption is that each time frame and its trajectory are known for a limited duration, and the MPC controller calculates the steering angle at the front to follow the path at the fastest entry speed on icy roads. Two approaches are proposed to solve this problem. One involves formulating the MPC problem using a nonlinear vehicle model, while the other entails the successive online linearization of the vehicle model. The paper includes discussions on computational complexity, as well as simulations of the proposed MPC controllers at velocities of 7 m/s and 21 m/s on slippery roads.**

***Index Terms*—Active steering, autonomous vehicles, model predictive control, nonlinear optimization, vehicle dynamics control, and vehicle stability.**

I. Introduction

The introduction of electronics, computers, and controls to enhance the overall system is causing a rapid shift and transformation in the automotive industry. The safety of the vehicle can be categorized into two types: passive safety and active safety. Passive safety deals with the build quality and robustness of the system at the manufacturing level. On the other hand, active safety is used to avoid accidents and facilitate the better controllability of vehicles in emergency situations, such as sudden exposure to slippery roads. The active safety systems available on the market are ABS (which improves braking efficiency) and traction control systems (which help prevent wheels from slipping and improve stability as well as steerability).

Additionally, the Active Front Steering (AFS) system uses the front steering command to reduce or destabilize forces from wind, asymmetric braking, and other sources to improve lateral vehicle stability[2]. Furthermore, by leveraging the installed cameras, sensors, and GPS, future systems are expected to offer sophisticated active safety techniques. Additionally, data sharing and communication among moving vehicles will enhance safety in hazardous driving situations. For instance, in slippery road conditions, information from leading vehicles can be shared, enabling other vehicles to assist the controller by providing additional data for improved performance.

In our discussion, we assume the availability of a trajectory planning system and focus on a double-lane changing scenario on a slippery road. In the analyzed paper, the primary emphasis is on controlling yaw and lateral vehicle dynamics through active front steering. The front steering angle serves as the input control, aiming to closely follow the intended path over a finite time horizon. Two types of AFS MPC problems are introduced and analyzed in the paper. The system's future evolution is initially predicted using a nonlinear vehicle model, and the MPC controller requires solving a nonlinear optimization problem at each time step. However, this poses a computational challenge and hinders experimental validation in a real-world system. The second formulation is based on the successive online linearization of the nonlinear vehicle model, linearizing it at each time step and creating a time-varying (LTV) system with a linear MPC controller. Finally, a single-step horizon LTV MPC is presented, which does not require complex optimization tools and can be adjusted for better performance.

II. Modeling

This section details the modeling of the vehicle and tire dynamics used for the controller design [3]. To simplify the representation, each pair of front and rear wheels of the car has been represented as a single wheel, resembling a bicycle. This simplification is referred to as the bicycle model as shown in Figure 1.

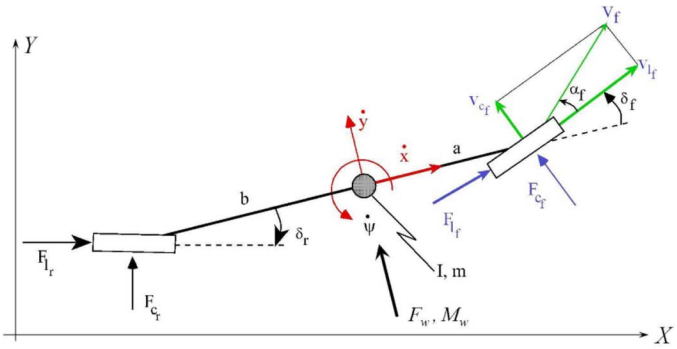

Fig. 1: Simplified vehicle "bicycle model".

F_l	Longitudinal (or "tractive") tire forces
F_c	lateral (or "cornering") tire forces
F_x, F_y	forces in car body frame
F_z	Normal tire load
I	Car inertia
(X, Y)	Absolute car position in inertial coordinates
l_f	distance of front wheels from the center of gravity
l_r	distance of rear wheels from the center of gravity
g	Gravitational constant
m	Car mass
R	Wheel radius

s	Slip ratio
(v_l, v_c)	Longitudinal and lateral wheel velocities
(x, y)	longitudinal and lateral coordinates in the car frame
$\dot{x}$	Vehicle speed
α	Slip angle
δ	Wheel steering angle
μ	Road friction coefficient
ψ	Heading angle
$(.)_f$	variable at the front wheel
$(.)_r$	variable at the rear wheel

Assuming that there is constant normal tire load, i.e., F_{z_f},F_{z_r} = constant, the following equations of dynamics are deduced from Figure 1.

$$\ddot{x} = \dot{y}\dot{\psi} + \frac{2(F_{x_f} + F_{x_r})}{m} \tag{1a}$$

$$\ddot{y} = -\dot{x}\dot{\psi} + \frac{2(F_{y_f} + F_{y_r})}{m} \tag{1b}$$

$$\ddot{\psi} = \frac{2(aF_{y_f} - bF_{y_r})}{I} \tag{1c}$$

The vehicle's equations of motion in an absolute inertial frame are

$$\dot{Y} = \dot{x}\sin(\psi) + \dot{y}\cos(\psi) \tag{2a}$$

$$\dot{X} = \dot{x}\cos(\psi) - \dot{y}\sin(\psi) \tag{2b}$$

Longitudinal and lateral tire forces which are formulated in III lead to the following forces acting on the center

$$F_y = F_l\sin(\delta) + F_c\cos(\delta) \tag{3a}$$

$$F_x = F_l\cos(\delta) - F_c\sin(\delta) \tag{3b}$$

Tire forces, $F_l = f_l(\alpha, s, \mu, F_z)$, and $F_c = f_c(\alpha, s, \mu, F_z)$, for each tire are the functions of slip angle (α), slip ratio (s) road friction coefficient (μ) and normal tire load (F_z). The slip ratio is defined as

$$s = \begin{cases} \frac{r\omega}{v} - 1 \text{ if } v > r\omega,\ v \neq 0 \text{ for braking} \\ 1 - \frac{r\omega}{v} \text{ if } v < r\omega,\ \omega \neq 0 \text{ for driving} \end{cases} \tag{4}$$

The slip angle represents the angle between the wheel velocity and the direction of the wheel itself:

$$\alpha = \tan^{-1}\frac{v_c}{v_l} \tag{5}$$

In equation 5, v_c and v_l are the lateral (or cornering) and longitudinal wheel velocities, respectively, which are expressed as

$$v_l = v_y\sin(\delta) + v_x\cos(\delta) \tag{6a}$$

$$v_c = v_y\cos(\delta) - v_x\sin(\delta) \tag{6b}$$

and

$$v_{y_f} = \dot{y} + a\dot{\psi} \qquad v_{y_r} = \dot{y} - b\dot{\psi} \tag{7a}$$

$$v_{x_f} = \dot{x} \qquad v_{x_r} = \dot{x} \tag{7b}$$

F_z is distributed between the front and rear wheels based on the geometry of the car model, described by the parameters a and b;

$$F_{z_f} = \frac{bmg}{2(a+b)} \tag{8a}$$

$$F_{z_r} = \frac{amg}{2(a+b)} \tag{8b}$$

Using the equations 1-8, the nonlinear vehicle dynamics can be described by the following compact differential equation assuming a **certain slip ratio** (s) and **friction coefficient value** (μ):

$$\dot{\xi} = f_{s,\mu}(\xi, u) \tag{9a}$$

$$\eta = h(\xi) \tag{9b}$$

where the state vector and the input vector are given by: $\xi = [y\ \dot{y}\ x\ \dot{x}\ \psi\ \dot{\psi}\ Y\ X]^T$ and $u = \delta_f$

The output map is given as

$$\eta = \begin{bmatrix} \psi \\ Y \end{bmatrix} = \begin{bmatrix} 0 & 0 & 0 & 1 & 0 & 0 & 0 \\ 0 & 0 & 0 & 0 & 0 & 1 & 0 \end{bmatrix} \xi \tag{10}$$

Nonlinear kinematic and dynamics equations of 2WS the vehicle can also be represented with control input, δ_f, as follows:

$$\dot{\xi}(t) = \begin{pmatrix} \dot{y} \Rightarrow & v\sin(\psi + \beta) \\ \ddot{y} \Rightarrow & -\dot{x}\dot{\psi} + \frac{2(F_{y_f} + F_{y_r})}{m} = \\ \dot{x} \Rightarrow & v\cos(\psi + \beta) \\ \ddot{x} \Rightarrow & \dot{y}\dot{\psi} + \frac{2(F_{x_f} + F_{x_r})}{m} \\ \dot{\psi} \Rightarrow & r \\ \ddot{\psi} = \dot{r} \Rightarrow & \frac{1}{I}(\alpha F_{y_f}\cos(\delta) - bF_{y_r}) \\ \dot{Y} \Rightarrow & \dot{x}\sin(\psi) + \dot{y}\cos(\psi) \\ \dot{X} \Rightarrow & \dot{x}\cos(\psi) - \dot{y}\sin(\psi) \end{pmatrix} \tag{11}$$

where $\beta = \tan^{-1}(\frac{b}{a+b}\tan(\delta_f))$ and acceleration of the car is constant, i.e. $\dot{v} = 0$. Forces in x- and y-directions, F_x and F_y, are the function of the forward steering angle, δ_f and longitudinal and lateral tire forces acting on the center.

III. Tire Model

Most of the forces except aerodynamic force and gravity that affect vehicle handling are produced by the tires. These forces, due to the complex and nonlinear way tires behave,

have the most significant impact on how a vehicle maneuvers both in a straight line and around corners. So, using an accurate and nonlinear tire model is crucial, especially when exploring extreme control inputs that push the vehicle near its limits. In these scenarios, the vehicle's lateral and longitudinal movements are strongly coupled through the tire forces, and it's common to have large values of slip ratio and slip angle happening simultaneously.

The paper has used the Pacejka Tire Model [4] to calculate the tire's longitudinal and cornering forces. This model is a complex, semi-empirical nonlinear formula that considers the interaction between longitudinal and cornering forces for combined steering and braking. Here, these forces are assumed to be dependent on slip angle, normal force, slip ratio fixed values of friction coefficients.

This formula has been derived from the experiments and each constant could represent a force that can be changed to fit the real factors into the model.

The basic form of each of the characteristics of large values the tire suggests the use of the sine function as a first step in developing the final formula.

$$F = D\sin(B\alpha) \tag{12}$$

with F standing for either side force, self-aligning torque, or break force and α denoting slip angle. e. In 12 D is the peak value and the product DB equals the slip stiffness at zero slip. Eq. 12 does not give a good representation for larger values of α. A gradually increasing extension of the X-axis appears to be necessary. To accomplish this, the $\arctan$ function has been used. The formula 12 now changes into:

$$F = D\sin(C\arctan(B\alpha)) \tag{13}$$

In Eq. (2) D is still the peak value, the slip stiffness at zero slip is now equal to the BCD (from now on called the stiffness). The coefficient C governs the shape of the curve. The value of C makes the curve look like a side force, brake force, or a self-aligning torque characteristic. With C determined by the shape and D determined by the peak value, only B is left to control the stiffness. Still Eq. 13 is not good enough to describe every possible measured characteristic. There may be a need for an additional coefficient which makes it possible to accomplish a local extra stretch or compression of the curve. The coefficient E has been introduced into the formula in such a way that stiffness and peak value remain unaffected.

$$F = D\sin(C\arctan(B\Phi)) \tag{14a}$$

$$\Phi = (1-E)\alpha + \frac{E}{B}\arctan(B\alpha) \tag{14b}$$

The influence of E on the side force characteristic has similar effects that occur with the self aligning torque and brake force characteristics. The result is an equation with four coefficients, which is able to describe all the measured characteristics. The four coefficients are:

- $B \Rightarrow$ stiffness factor
- $C \Rightarrow$ shape factor
- $D \Rightarrow$ peak factor
- $E \Rightarrow$ curvature factor

To reduce the total number of quantified coefficients and to be able to calculate forces and torques at vertical loads which are different from the values used in the measurements, it is necessary to include the vertical load explicitly in the formula. To do so, the coefficients have to be written as a function of the vertical (normal) load, F_z. The peak factor, D, as a function of F_z may be approximately represented by the relationship:

$$D = a_1{F_z}^2 + a_2F_z \tag{15}$$

For the stiffness BCD of the side force characteristic (cornering stiffness), the formula is written as

$$BCD = a_3\sin(a_4\arctan(a_5F_z)) \tag{16}$$

and for the stiffness of both brake force (longitudinal slip stiffness) and self aligning torque (aligning stiffness) characteristics, the approximation is:

$$BCD = \frac{a_3{F_z}^2 + a_4F_z}{e^{a_5F_z}} \tag{17}$$

The shape factor, C, appears to be practically independent of F_z. For above mentioned force types C takes the following values:

- the side force : $C = 1.30$
- the brake force : $C = 1.65$
- the self aligning torque : $C = 2.40$

The stiffness factor B is found by stiffness by the shape and the peak factor.

$$B = \frac{BCD}{CD} \tag{18}$$

Finally, the curvature factor E as a function of F_z is given by:

$$E = a_6{F_z}^2 + a_7F_z + a_8 \tag{19}$$

Final Longitudinal and lateral equations of tire model:

1) Longitudinal Force, F_l:

$$F_l = D\sin(C\arctan(B\Phi)) + \Delta S_v \tag{20a}$$

$$\Phi = (1-E)(\sigma + \sigma S_h) + (E/B)\arctan(B(\sigma + \Delta S_h)) \tag{20b}$$

$$D = a_1{F_z}^2 + a_2F_z \tag{20c}$$

$$C = 1.30 \tag{20d}$$

$$B = \left(\frac{a_3\sin(a_4\arctan(a_5F_z)}{CD}\right)(1 - a_{12}|\gamma|) \tag{20e}$$

$$E = a_6{F_z}^2 + a_7F_z + a_8 \tag{20f}$$

$$\Delta S_h = a_9\gamma \tag{20g}$$

$$\Delta S_v = (a_{10}{F_z}^2 + a_{11}F_z)\gamma \tag{20h}$$

2) Lateral Force, F_c:

$$F_c = D\sin(C\arctan(B\Phi)) + \Delta S_v \tag{21a}$$
$$\Phi = (1-E)\alpha + (E/B)\arctan(B\alpha) \tag{21b}$$
$$D = a_1 {F_z}^2 + a_2 F_z \tag{21c}$$
$$C = 1.65 \tag{21d}$$
$$B = \frac{a_3 {F_z}^2 + a_4 F_z}{CDe^{a_5 F_z}} \tag{21e}$$
$$E = a_6 {F_z}^2 + a_7 F_z + a_8 \tag{21f}$$
$$\Delta S_h = a_9 \gamma \tag{21g}$$
$$\Delta S_v = (a_{10} {F_z}^2 + a_{11} F_z)\gamma \tag{21h}$$

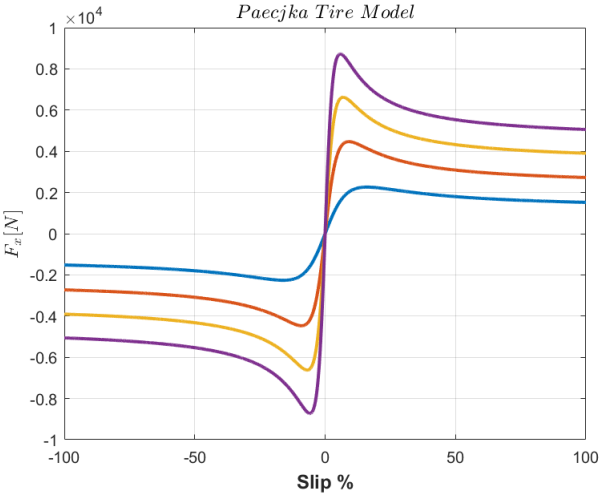

Fig. 2: Longitudinal Tire Forces at μ [0.1 0.3 0.5 0.7]

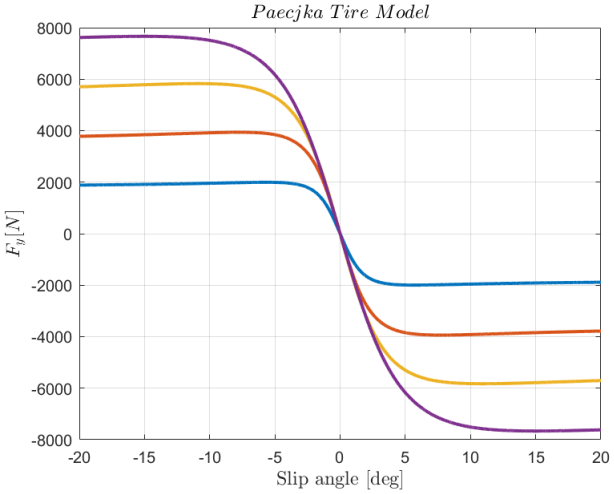

Fig. 3: Lateral Tire Forces at μ [0.1 0.3 0.5 0.7]

Figures 2 and 3 represent the longitudinal and lateral forces versus longitudinal slip and slip angle, for fixed values of the friction coefficients calculated from the formulae 21 and 22.

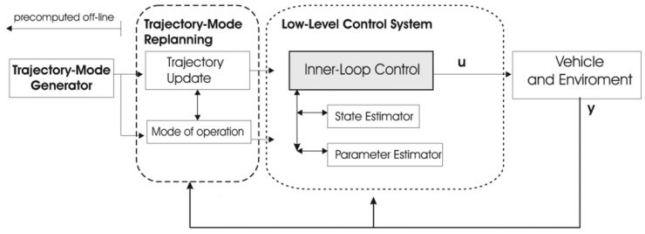

Fig. 4: Architecture for fully autonomous vehicle guidance system.

IV. Hierarchical Framework for Autonomous Vehicle Guidance

In this section, the authors introduce a schematic architecture (Fig. 4) borrowed from the aerospace field to illustrate their approach and contributions in the context of an autonomous vehicle guidance system. The architecture comprises four modules: the trajectory/mode generator, trajectory/mode replanning, low-level control system, and vehicle/environmental model. The trajectory/mode planning module precomputes the vehicle trajectory, including timing and conditions for operation mode changes. Examples of operation mode changes include parachute deployment in aerospace or switching between energy sources like gas, electricity, or hydrogen in automotive scenarios.

The trajectory and mode of operation, initially computed offline, can be recalculated online during the drive by the trajectory/mode replanning module based on real-time measurements or specific events like tracking errors or hardware failures. The low-level control system commands various vehicle actuators, such as steering angles, brakes, engine torque, and suspensions, using information from sensors, states, and parameters provided by the trajectory/mode replanning module. The primary objective of the low-level control system is to keep the vehicle as close as possible to the planned trajectory despite factors like measurement noise, uncertainties, and sudden changes in vehicle and road conditions. The section emphasizes the importance of considering additional vehicle dynamic states, especially when operating near the stability limit, to effectively handle disturbances such as tire saturation and ensure stable vehicle maneuvering.

The presented framework, illustrated in Figure 4, outlines the essential components of an autonomous vehicle guidance system, encompassing the trajectory/mode generator, trajectory/mode replanning, low-level control system, and the vehicle and environmental model. Acknowledging the oversimplification of this scheme, the authors recognize the potential existence of additional hierarchical levels within the trajectory/mode re-planning and low-level control system modules, collectively referred to as the guidance and navigation control (GNC) system. Notably, these modules operate with differing information on the environment and vehicle, and their execution frequencies vary. The design incorporates vehicle and environment models of varying detail, with control

paradigms exploring the use of high-fidelity vehicle models for lower-level controllers and less detailed models for trajectory planning. The study highlights the diversity in GNC algorithms concerning focus, vehicle dynamical model, control design, and sensor choices through the discussion of specific examples from related literature, ultimately setting the stage for a more detailed exploration of the specific scenario involving an active steering system in subsequent sections.

The paper explores two methods for path generation. In the first method, the trajectory is formed by slowly driving a test vehicle along the desired path, such as a double-lane change maneuver. The actual path is recorded by differential GPS and utilized as the desired path for subsequent tests at higher speeds. This approach, previously used for generating a reference path for a steering robot on high, eliminates the need for trajectory re-planning. It contributes to facilitating systematic and repeatable tests of safety-critical emergency maneuvers under limit conditions, like obstacle avoidance on slippery surfaces such as snow and ice. In the second method, assuming the availability of a trajectory re-planning module, the trajectory is recomputed at a lower frequency than the lower-level controller. The focus in both cases is on the lower-level control design, employing nonlinear and Time-Varying Model Predictive Control (MPC) for the specific scenario of an active steering system.

As discussed, the challenge involved in obtaining steering desired to accomplish the limit maneuver while maintaining stability.The approach is characterized by several key features. Firstly, it is model-based, relying on the vehicle model and incorporating the highly nonlinear Pacejka tire model detailed in Section III. Secondly, the approach includes constraints on inputs and states as part of the control design. Thirdly, it is systematic and versatile, capable of handling multiple variables, and adaptable to accommodate new actuators and higher fidelity models. These aspects collectively contribute to the robustness and flexibility of the approach in the context of active steering system control.

V. Design of Active Steering Controller

In this section, we present the control design methodology for addressing the path following problem using an active steering system[5] . The desired references for the heading angle (ψ), yaw rate($\dot{\psi}$),and lateral distance Y define a specific path over a finite horizon. Leveraging the nonlinear vehicle dynamics and the Pacejka tire model, we predict the vehicle's behavior, with the front steering angle (δ_f) chosen as the control input. The rear steering angle is assumed to be zero $\delta_r = 0$, and tire slip ratios s_f and s_r are measured, while road friction μ is estimated at each time instant.

The path following problem is tackled using a Model Predictive Control (MPC) scheme, a technique that utilizes a model of the plant to forecast the future system evolution. At each sampling time, an open-loop optimal control problem is solved over a finite horizon, minimizing the deviations of predicted outputs from their references. The resulting optimal control signal is then applied to the system during the subsequent sampling interval. This process repeats at each time step, considering new measurements of the state.

Two formulations of the Active Front Steering (AFS) MPC problem are introduced. The first formulation, detailed in Section V-A, employs the nonlinear vehicle model and the Pacejka tire model for predicting the system's future evolution. The optimization problem involved is nonlinear and solved online at each time step. The second formulation, discussed in Section V-B, addresses computational challenges by using a Linear Time-Varying (LTV) approximation of the vehicle model. This results in a suboptimal LTV MPC controller, where a time-varying convex quadratic optimization problem is formulated and solved at each time step. The inclusion of a tire slip angle constraint is shown to enhance MPC performance, particularly in stabilizing the vehicle at high speeds.

A. Nonlinear(NL) MPC

To obtain a finite-dimensional optimal control problem, we discretize the system dynamics(9) with a fixed sampling time.

$$\xi(k+1) = f_{s,\mu}^{dt}(\xi(k), u(k)) \tag{22a}$$

$$\eta(k) = h(\xi(k)) \tag{22b}$$

where the Δu formulation is used, i.e., $u(k) = u(k-1) + \Delta u(k)$ and $u(k) = \delta_f(k)$, $\Delta u(k) = \Delta\delta_f(k)$. The objective or the cost function of the system can be defined as follows:

$$\begin{aligned} J(\xi(k), \Delta U_t) &= \sum_{i=1}^{H_p} (\hat{\eta}_{t+i,t} - \eta_{ref_{t+i,t}})^T \, Q \, (\hat{\eta}_{t+i,t} - \eta_{ref_{t+i,t}}) \\ &+ \sum_{i=0}^{H_c-1} \Delta u_{t+i,t} \, R \, \Delta u_{t+i,t} \\ &= \sum_{i=1}^{H_p} \Big[\Big] \hat{\eta}_{t+i,t} - \eta_{ref_{t+i,t}}{}_Q^2 + \sum_{i=0}^{H_c-1} \Big[\Big] \Delta u_{t+i,t}{}_R^2 \end{aligned} \tag{23}$$

In eq.23 the first summand reflects the desired performance on target tracking, the second summand is a measure of the steering effort. At each time step t the following finite horizon optimal control problem is solved:

$$\begin{aligned} \min_{\Delta U} \quad & J(\xi(k), \Delta U_t) \\ \text{st.} \quad & \xi(k+1) = f_{s,\mu}^{dt}(\xi(k), u(k)), \;\; k = t, \ldots, t + H_p \\ & \eta(k) = h(\xi(k)), \;\; k = t, \ldots, t + H_p \\ & \delta_{f,min} \leqslant u_{k,t} \leqslant \Delta\delta_{f,max} \;\; k = t, \ldots, t + H_c - 1 \\ & \Delta\delta_{f,min} \leqslant \Delta u_{k,t} \leqslant \Delta\delta_{f,max} \;\; k = t, \ldots, t + H_c - 1 \\ & u_{k,t} = u_{k,t-1} + \Delta u_{k,t} \end{aligned} \tag{24}$$

When the above optimization problem is solved at time t for the current observed states $\xi_{t,t}$, sequence of the optimal control inputs, $\Delta U_t^* = [\Delta u_{t,t}^*, \ldots, \Delta u_{t+H_c-1,t}^*]^T$, within the specified control horizon. The resulting state feedback control law is,

$$\delta_f(t) = \delta_f(t-1) + \Delta u_{t,t}^* \tag{25}$$

At the next time step $t+1$, the optimization problem is solved over a shifted horizon based on the new measurements of the state.

B. LTV MPC

LTV MPC is a control technique that can be used to control systems that change over time. It works by predicting the future behavior of the system and then optimizing the control inputs to achieve the desired objectives. From the above non-linear dynamical system in the following form:

$$\dot{\xi} = f(\xi, u)$$
$$y = h(\xi)$$

we consider small changes in the system states, inputs, and outputs around a trajectory given by $\xi_0(t), u_0(t), y_0(t)$:

$$\xi(t) = \xi_0(t) + \delta\xi(t)$$
$$u(t) = u_0(t) + \delta u(t)$$
$$y(t) = y_0(t) + \delta y(t)$$

If the $\delta\xi(t)$, $\delta u(t)$, $\delta y(t)$ changes are small enough, we can obtain a linearized system around the $\xi_0(t)$, $u_0(t)$, $y_0(t)$ trajectory in the following way:

$$\delta\dot{\xi} = \left.\frac{\partial f(\xi,u)}{\partial\xi}\right|_{\substack{\xi=\xi_0(t)\\u=u_0(t)}}\delta\xi + \left.\frac{\partial f(\xi,u)}{\partial u}\right|_{\substack{\xi=\xi_0(t)\\u=u_0(t)}}\delta u$$
$$\delta y = \left.\frac{\partial h(\xi)}{\partial\xi}\right|_{\xi=\xi_0(t)}\delta\xi$$

Using the above linearized system, we can construct a quadratic programming-based MPC, which uses an LTV prediction model. Let A_k, B_k, C_k, D_k denote the discrete-time state matrices of the vehicle model linearized at $t = kT_s$. By using successive substitution, it is straightforward to derive the prediction model [6] of performance outputs (signals of interest) over the prediction horizon.

The objective function of the LTV MPC controller: let t be the current time and $\xi(t)$ be the current state and $u(t-1)$ be the previous input of system.

$$\min_{\Delta u_t,\epsilon} \sum_{i=1}^{Hp} \|\delta\eta_{t+i,t} - \delta\eta_{ref_t+i,t}\|_Q^2 + \sum_{i=0}^{H_c-1} \|\delta u_{t+i,t}\|_R^2 + \rho\epsilon \tag{26a}$$

$$\delta\xi_{k+1,t} = A_t\delta\xi_{k,t} + B_t\delta u_{k,t} \tag{26b}$$
$$\delta\alpha_{k,t} = C_t\delta\xi_{k,t} + D_t\delta \tag{26c}$$
$$\delta\eta_{k,t} = \begin{bmatrix}0&0&1&0&0&0\\0&0&0&1&0&0\\0&0&0&0&1&0\end{bmatrix}\delta\xi_{k,t} \tag{26d}$$
$$Herek = t, ...t + H_p$$
$$u_{k,t} = u(t-1) + \delta u_{k,t} \tag{26e}$$
$$u_{t-1,t} = u(t-1) \tag{26f}$$
$$\Delta u_{k,t} = u_{k,t} - u_{k-1,t} \tag{26g}$$
$$\delta_{f,min} <= u_{k,t} <= \delta_{f,max} \tag{26h}$$
$$Herek = t, ..., t + H_c - 1$$
$$\delta\alpha_min - \epsilon <= \delta\alpha_{k,t} <= \delta\alpha_{max} + \epsilon, \tag{26i}$$
$$k = t + H_c, ...t + H_p \tag{26j}$$
$$\epsilon >= 0 \tag{26k}$$
$$\delta\xi_{t,t} = 0 \tag{26l}$$

Here $\Delta u_t = [\delta u_{t,t}, ..., \delta u_{t+H_c-1,t}]'$ and model (26b) and (26c) are obtained by the linearizing model (22) at each time step t around $\eta(t), u(t-1)$.
$\delta\eta = [\delta\psi, \delta\dot{\psi}, \delta Y]$ denote the output of the linearized system.
$\delta\eta_ref$ denotes reference signal.
$\delta\alpha$ denotes the tire slip angle variation and it is considered as an additional output in the linearized model which is constrained and not tracked.
ϵ is a slack variable.
$\rho\epsilon$ penalizes the violation of the constraint on the slip angle and ρ is a weight coefficient.
The optimization problem can be written as a quadratic program as explained in (ltv starting eqn non). We denote by $\Delta u_t^* = [\delta u_{t,t}^*, ..., \delta u_{t+H_{c-1},t}^*]'$ the optimal sequence input deviations computed at time t by solving (26) for current observed states $\xi(t)$. Then, the first sample of Δ_t^* is used to compute the resulting state feedback control law is

$$u(t, \xi(t)) = u(t-1) + \delta u_{t,t}^*(t, \xi(t)). \tag{27}$$

- At the next time step $t+1$, the optimization problem (26) is solved over a shifted horizon based on an updated linear model (26b-26d) computed by linearizing the nonlinear vehicle model.
- Model (22) is linearized around a non-equilibrium operating point. The Linear Time-Invariant (LTI) model (26b)-(26d) at time t is utilized to predict state and output deviations from trajectories $\hat{\xi}_t(k)$, $\hat{\alpha}_t(k)$, $\hat{\eta}_t(k)$ for $k = t, \ldots, t + H_p$. These trajectories are obtained by solving (22) with $\xi(t)$ as the initial condition and $u(k) = u(t-1)$ for $k = t, \ldots, t + H_p$.
- The optimization variables $[\delta u_{t,t}, \ldots, \delta u_{t+H_c-1,t}]$ represent input variations relative to the previous input $u(t-1)$.
- Alternatively, the vehicle model (22) can be linearized around a nominal input $u_{\text{nom}}(k)$ and state trajectory $\xi_{\text{nom}}(k)$.
- In this linearization, equation (26e) becomes $u_{k,t} =$

$u_{\text{nom}}(k)+\delta u_{k,t}$, where $[\delta u_{t,t}, \ldots, \delta u_{t+H_c-1,t}]$ represents input variations around the nominal input.

- This approach requires a nominal input and state trajectory, denoted as $u_{\text{nom}}(k)$ and $\xi_{\text{nom}}(k)$. These trajectories could be obtained from the higher-level replanning algorithm in Section IV or from the lower-level MPC controller.
- It's emphasized that using this approach involves employing a Linear Time-Varying (LTV) model over the prediction horizon $(A_{t,k}, B_{t,k}, C_{t,k}, D_{t,k})$ for $k = t, \ldots, t + H_p - 1$ at each time step t, instead of the Linear Time-Invariant (LTI) model (26b)–(26d).

The discussed Model Predictive Control (MPC) scheme involves employing a Linear Time-Invariant (LTI) model for prediction over a horizon. Variations in the LTI model are managed through scheduling parameters based on flight conditions. The computational load for the proposed MPC includes solving the optimization problem (26) and incorporating the linear models (A_t, B_t, C_t, D_t) while translating it into a quadratic programming (QP) problem. The stability of the presented control scheme is a challenging topic, particularly in the face of model mismatch and uncertainties in tire characteristics and road conditions. The introduction of state constraints (26j) in the MPC scheme, a key contribution of this paper, is crucial for achieving acceptable performance, preventing instability, and addressing the limitations of a simple linear tire model. The constraints ensure operation within a mostly linear region of the tire force characteristic. Notably, these constraints are handled effectively in an MPC framework, utilizing a soft constraint formulation. The explicit inclusion of a tracking error on the yaw rate in the MPC performance index enhances the controller's performance based on extensive simulations.

VI. Double lane changing on Snow using Active Steering

The controllers above have been developed to study and implement the double-lane-changing maneuver that can be used for obstacle avoidance emergency maneuvers in which the vehicle is entering a double-lane change maneuver on snow or ice with a given initial forward speed. The control input is the front steering angle and the goal is to follow the trajectory as closely as possible by minimizing the vehicle deviation from the target path. The experiment is repeated with increasing entry speeds until the vehicle loses control. To best study the results, a reference trajectory has been generated that takes the current longitudinal position into account and outputs a reference lateral position and yaw angle. The main aim of the controllers is to follow the reference trajectory as closely as possible. The equations to calculate the lateral position Y and yaw angle ψ are given as follows:

$$Y_{ref} = \frac{d_{y_1}}{2}(1+\tanh(z_1)) - \frac{d_{y_2}}{2}(1+\tanh(z_2)) \tag{28a}$$

$$\psi_{ref} = \arctan\left(d_{y_1}\Big(\frac{1}{\cosh(z_1)}\Big)^2\Big(\frac{1.2}{d_{x_1}}\Big) - d_{y_2}\Big(\frac{1}{\cosh(z_2)}\Big)^2\Big(\frac{1.2}{d_{x_2}}\Big)\right) \tag{28b}$$

$$z_1 = \frac{2.4}{d_{x_1}}(X - X_{s_1}) - \frac{2.4}{2} \tag{28c}$$

$$z_2 = \frac{2.4}{d_{x_2}}(X - X_{s_2}) - \frac{2.4}{2} \tag{28d}$$

where $d_{x_1} = 25$, $d_{x_2} = 21.95$, $d_{y_1} = 4.05$, $d_{y_2} = 5.7$, $X_{s_1} = 27.19$ and $X_{s_2} = 56.46$. The above parameters have been used for NLMPC and LTV-MPC controllers.

VII. Presentation and Discussion of Results

This section presents the results of three controllers that have been mentioned above in Section V. As per the original paper, the three controllers will be mentioned as A, B, and C respectively.

A. Controller A: Non-linear MPC

The following parameters have been used to implement the non-linear mpc controller:

$T = 0.05s$, $H_p = 7, H_c = 3$, $\delta_f, min = -10^\circ$, $\delta_f, max = 10^\circ$, $\triangle\delta_f, min = -1.5^\circ$, $\triangle\delta_f, max = 1.5^\circ$, $\mu = 0.3$,
$Q = \begin{pmatrix} 500 & 0 \\ 0 & 75 \end{pmatrix}$, $R = 150$

To address the non-linear optimization problem, we employed the FMINCON solver in MATLAB due to its availability and ease of use. We assumed slow entry speeds, as specified in the original paper, reflecting the limited computational capacity of the real hardware used in experiments. The increase in entry speeds necessitates higher control and prediction horizons for a seamless path prediction. However, optimizing at higher speeds requires more computation, which is currently unattainable.

By comparing the lateral position and yaw angle in our simulation and the original simulation for nlmpc controller with entry speed at 7 m/s and μ = 0.3, the tracking errors Y_{rms} = 0.0481 and ψ_{rms} = 0.055 are very small. The original simulation tracking errors are Y_{rms} = 0.00481 and ψ_{rms} = 0.153.

Figure 5 and 6 represent the controller behavior at 7 m/s and 21 m/s entry speeds respectively. We can observe that the performance of the nonlinear MPC controller is significantly different at entry speeds of 7 m/s and 21 m/s. At 7 m/s, the controller is able to track the desired yaw rate with a small overshoot and keep the front slip angle within the desired bounds. However, at 21 m/s, the yaw rate overshoot is much

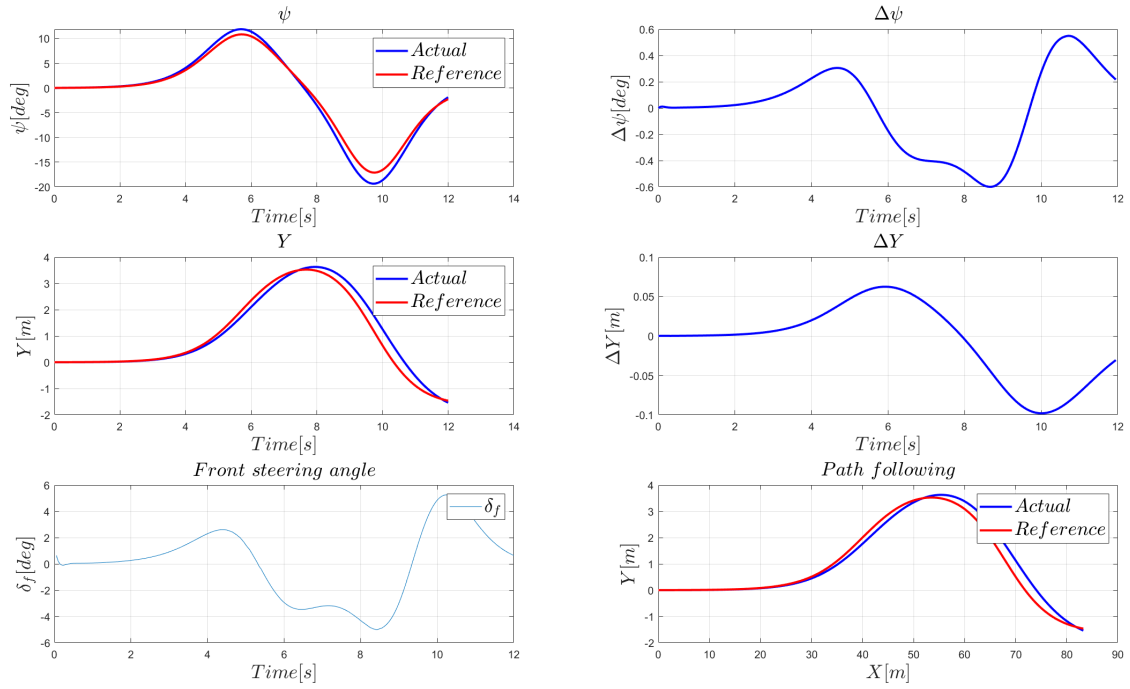

Fig. 5: Simulation results at 7-m/s entry speed with Controller A - NL MPC

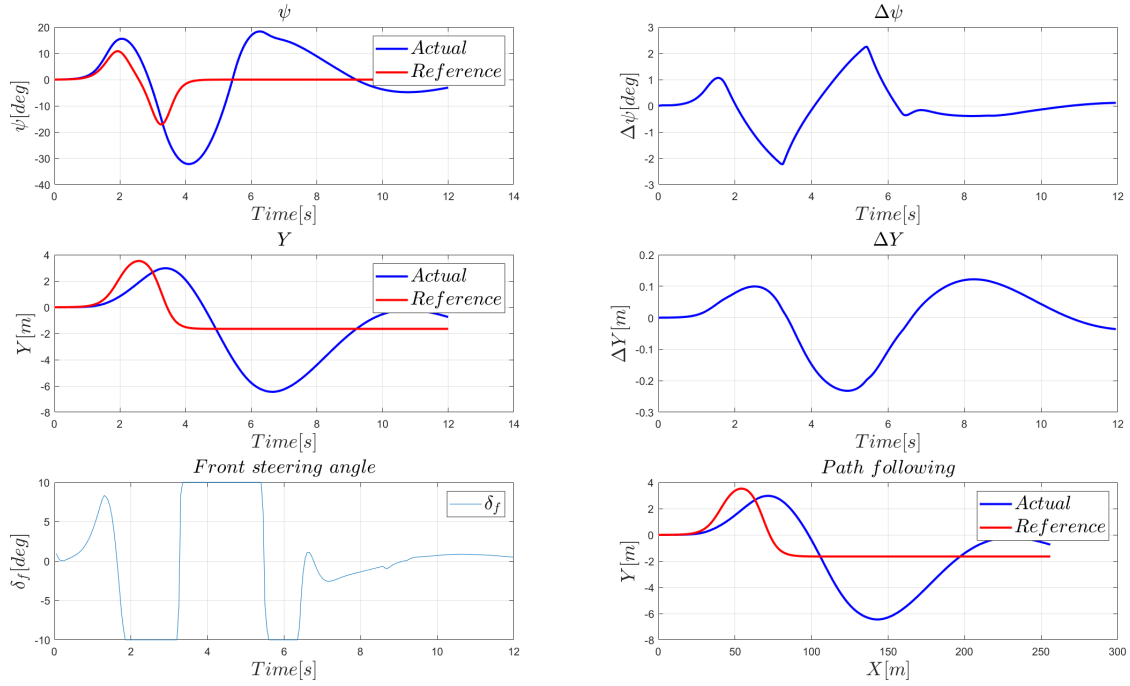

Fig. 6: Simulation results at 21-m/s entry speed with Controller A - NL MPC

larger, and the controller takes longer to settle. Additionally, the front slip angle reaches the upper bound for a brief period of time at 21 m/s. The computation time for the MPC controller is also higher at 21 m/s than at 7 m/s.

Overall, the nonlinear MPC controller provides good performance at both 7 m/s and 21 m/s, but the performance is significantly better at 7 m/s. This is because the controller has to deal with more challenges at 21 m/s, such as increased momentum and lateral force requirements.

B. Controller B : LTV MPC

The following parameters has been used to implement the ltv mpc controller:

$T = 0.05s$, $H_p = 25, H_c = 10$, $\delta_f, min = -10^\circ$, $\delta_f, max = 10^\circ$, $\triangle\delta_f, min = -0.85^\circ$, $\triangle\delta_f, max = 0.85^\circ$, $\mu = 0.3$, $\alpha_m in = -2.2^\circ$, $\alpha_m ax = 2.2^\circ$,
$Q = \begin{pmatrix} 500 & 0 & 0 \\ 0 & 10 & 0 \\ 0 & 0 & 10 \end{pmatrix}$, $R = 50000$,$\rho = 1000$

LTV MPC has been implemented by linearizing the non-linear function obtained from the vehicle dynamics equations. At each time step, the linear model is obtained by analytic differentiation of the nonlinear vehicle model and a numeric linearization of the Pacejka tire model.

From the figures 7 and 8 the LTV-MPC controller performs better at an entry speed of 10 m/s than at an entry speed of 21 m/s. The yaw rate tracking is more accurate, with less overshoot and settling time at 10 m/s. The front slip angle is also better controlled at 10 m/s, staying within the desired bounds at all times. In contrast, the front slip angle reaches the upper bound for a brief period of time at 21 m/s.

The computation time for the LTV-MPC controller is also shorter at 10 m/s than at 21 m/s. This is because the controller has to optimize over a longer horizon at 21 m/s to account for the increased momentum of the vehicle.

Overall, the LTV-MPC controller provides better performance at 10 m/s than at 21 m/s. This is because the controller has to deal with more challenges at 21 m/s, such as increased momentum and lateral force requirements. However, the LTV-MPC controller is still able to provide good performance at 21 m/s, making it a promising approach for vehicle control at high speeds.

C. Controller C : LTV MPC - II

This controller is similar to Controller B but with the control horizon $H_c = 1$.

The following parameters has been used to implement the non-linear mpc controller:

$T = 0.05s$, $H_p = 7, H_c = 3$, $\delta_f, min = -10^\circ$, $\delta_f, max = 10^\circ$, $\triangle\delta_f, min = -1.5^\circ$, $\triangle\delta_f, max = 1.5^\circ$, $\mu = 0.3$,
$Q = \begin{pmatrix} 500 & 0 \\ 0 & 75 \end{pmatrix}$, $R = 150$

Controller C at 17 m/s has a similar yaw rate tracking performance to the LTV-MPC controller at 10 m/s. Both controllers are able to track the desired yaw rate with very little overshoot or settling time. However, Controller C has slightly better front slip angle control than the LTV-MPC controller at 10 m/s. This is because the Controller C setting results in a more aggressive controller that is better able to keep the front slip angle within the desired bounds.

Controller C also has a shorter computation time than the LTV-MPC controller at 10 m/s. This is because the Controller C setting reduces the complexity of the optimization problem that the controller has to solve.

Compared to the NL-MPC controller at 17 m/s, Controller C has significantly better yaw rate tracking and front slip angle control performance. The NL-MPC controller has a large overshoot and settling time in the yaw rate response, and the front slip angle reaches the upper bound for a significant period of time. Controller C, on the other hand, is able to track the desired yaw rate and front slip angle with much better accuracy and precision.

Controller C also has a shorter computation time than the NL-MPC controller at 17 m/s. This is because Controller C uses a simplified model of the vehicle dynamics, which makes the optimization problem easier to solve.

Overall, Controller C is a better choice than the NL-MPC controller for vehicle control at 17 m/s. It has better yaw rate tracking and front slip angle control performance, and it has a shorter computation time.

VIII. Conclusion

In conclusion, our investigation into the application of Model Predictive Control (MPC) for Active Front Steering (AFS) in autonomous vehicles has provided valuable insights into control strategies and their implications. Our study primarily compared the effectiveness of Nonlinear MPC (NL-MPC) and Linear Time-Varying MPC (LTV-MPC) in managing the complexities of trajectory tracking under diverse conditions.

Both NL-MPC and LTV-MPC showcased commendable performance in trajectory tracking, yet their strengths emerged under different scenarios. NL-MPC demonstrated efficiency at moderate speeds, providing precise control within computational limits. However, challenges arose at higher speeds, emphasizing the need for enhanced computational capabilities. On the other hand, LTV-MPC exhibited robustness, particularly at elevated speeds, showcasing its adaptability to real-world applications.

The Pacejka tire model was used to simulate the complex behavior of tires, which was crucial in determining the lateral and longitudinal dynamics. Precise tire modeling was essential for attaining exact control, particularly when the vehicle is getting close to its limits. The study taught us how important non-linear and realistic tire models are to improving the control systems of autonomous vehicles.

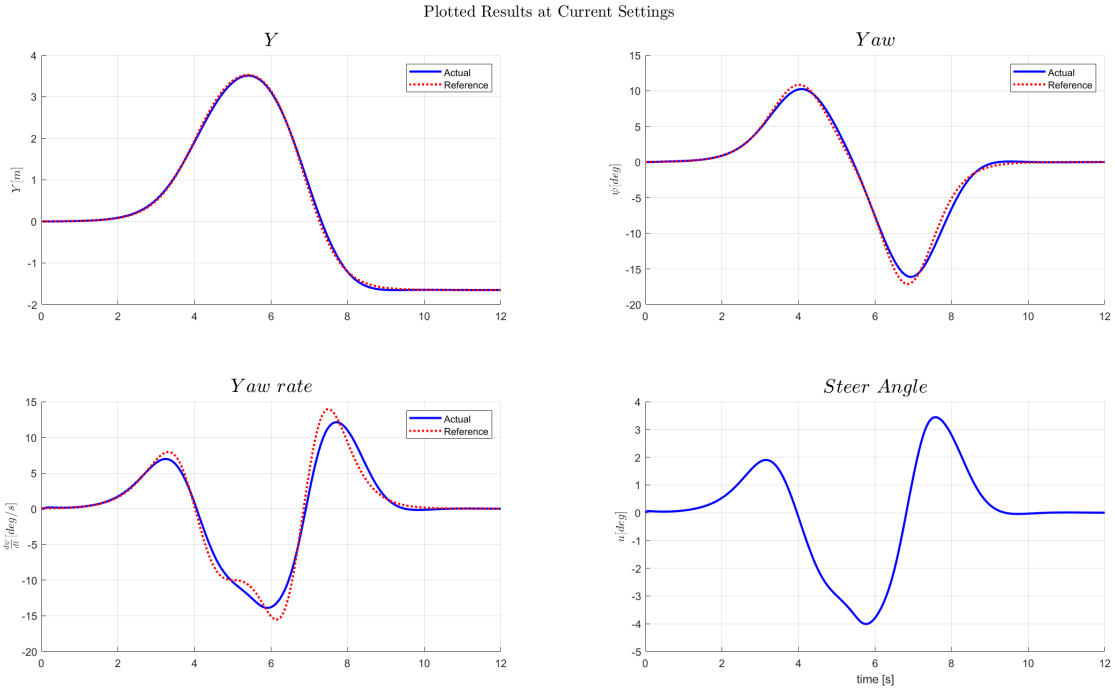

Fig. 7: Simulation results at 10-m/s entry speed with Controller B - LTV MPC

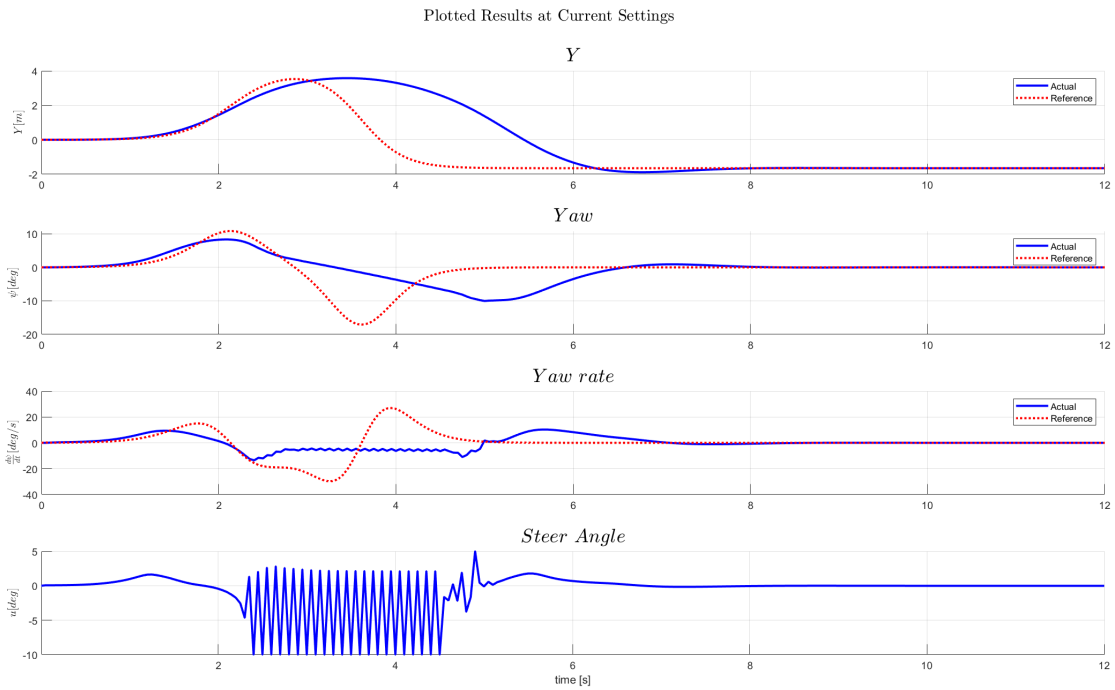

Fig. 8: Simulation results at 21-m/s entry speed with Controller B - LTV MPC

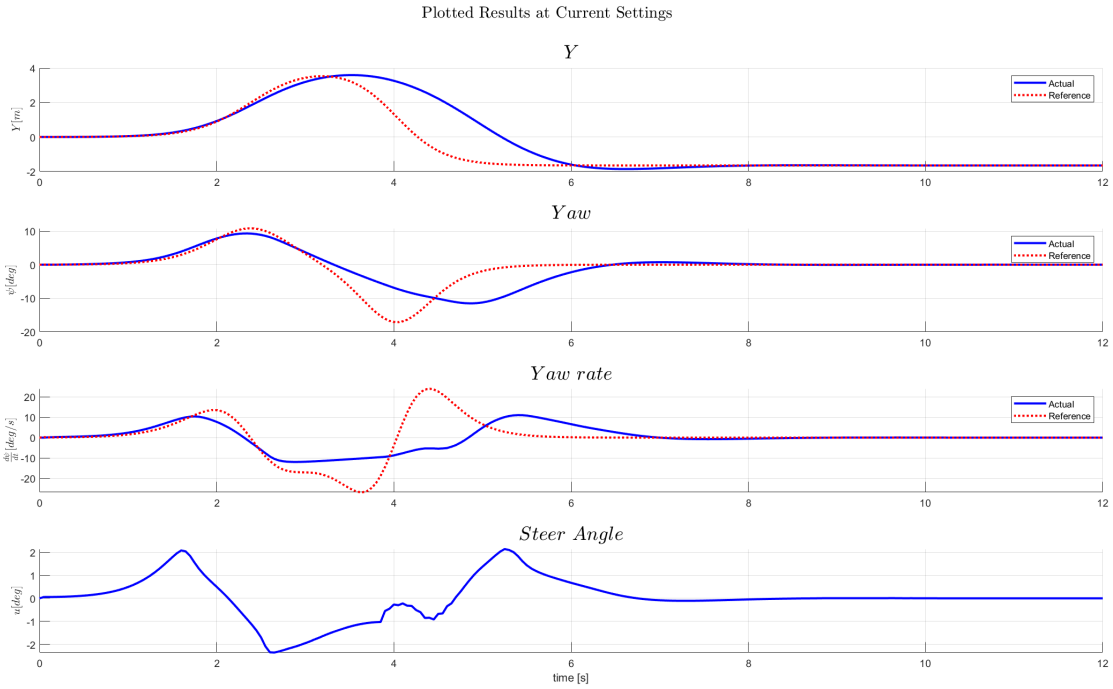

Fig. 9: Simulation results at 17-m/s entry speed with Controller C

This project has been valuable in improving our understanding of advanced vehicle control systems, specifically focusing on Active Front Steering (AFS) through Nonlinear Model Predictive Control (NL-MPC) and Linear Time-Varying MPC (LTV-MPC).We've learned how tire modeling, computational complexity, and practical adaptability are closely connected. The project highlighted the importance of accuracy, speed, and the need for ongoing technological advancements.Additionally, the difficulties we faced emphasized the need to improve control strategies, especially for self-driving cars. This also points to opportunities for future research and advancements in this field.

REFERENCES

1 Falcone, P., Borrelli, F., Asgari, J., Tseng, H. E., and Hrovat, D., "Predictive active steering control for autonomous vehicle systems," *IEEE Transactions on Control Systems Technology*, vol. 15, no. 3, pp. 566–580, 2007.

2 Ackermann, J., Bünte, T., and Odenthal, D., "Advantages of active steering for vehicle dynamics control," 1999. [Online]. Available: https://api.semanticscholar.org/CorpusID:17257332

3 Kong, J., Pfeiffer, M., Schildbach, G., and Borrelli, F., "Kinematic and dynamic vehicle models for autonomous driving control design," in *2015 IEEE Intelligent Vehicles Symposium (IV)*, 2015, pp. 1094–1099.

4 Pacejka, H. B., "Modelling of tyre force and moment generation," in *Rolling Contact Phenomena*, Jacobson, B. and Kalker, J. J., Eds. Vienna: Springer Vienna, 2000, pp. 277–327.

5 Rajamani, R., *Vehicle Dynamics and Control*, ser. Mechanical Engineering Series. Springer US, 2011. [Online]. Available: https://books.google.com.tr/books?id=cZJFDox4KuUC

6 Velhal, S. and Thomas, S., "Improved ltvmpc design for steering control of autonomous vehicle," *Journal of Physics: Conference Series*, vol. 783, no. 1, p. 012028, jan 2017. [Online]. Available: https://dx.doi.org/10.1088/1742-6596/783/1/012028